Cyclic Voltammetry at Monolayer Covered Electrodes: The Effect of Monolayers on the Reduction of Cytochrome *c*

Michael J. Honeychurch*,† and Garry A. Rechnitz

Department of Chemistry, University of Hawaii, 2545 The Mall, Honolulu, Hawaii, 96822

Received: February 28, 1997; In Final Form: June 2, 1997[⊗]

A theory is presented to account for the characteristics of cyclic voltammograms (CVs) at monolayer covered electrodes. It is shown that CVs of reversible systems can exhibit peak separations of greater than 57/*n* mV, a characteristic previously associated with quasi-reversible systems. In the presence of a monolayer, the dimensionless current function is less than the value for an ideal reversible reaction at a bare electrode. The theory was tested experimentally for the reduction of cytochrome *c* at a 4,4′-bipyridal disulfide-modified gold electrode. A good correspondence was obtained between predicted (68 mV) and experimental (69 ± 4 mV) peak separations. The value of the diffusion coefficient of cytochrome *c* calculated from a plot of current vs sweep rate was 10.2×10^{-7} cm^2 s^{-1}, which is in good agreement with literature values. In contrast, using the traditional CV model for a bare electrode, the diffusion coefficient was calculated as 8.8×10^{-7} cm^2 s^{-1}.

Introduction

The reduction of cytochrome *c* has been studied extensively in the last 20 years at gold, metal oxide, glassy carbon, platinum, and edge plane graphite electrodes. [1−3] It is generally recognized that in order to promote electron transfer between cytochrome *c* and metal electrodes the addition of a promoter is necessary. [3] The promoter is not electroactive in the potential range of interest, so its function is different from that of mediators. In order to promote the electrochemistry of cytochrome *c* at gold electrodes, bifunctional promoters are considered necessary[4] unless rather extreme surface cleaning and pretreatment procedures are followed.[5] One part of the promoter molecule, typically a thiol or disulfide group, binds to the electrode, thus providing an adsorbed layer of promoter. The second functional part of the promoter, typically a weak base, is oriented toward the bulk solution and provides a site for electrostatic interaction with cytochrome *c*. The interaction between the basic groups of the modified electrode is thought to be with the lysine groups surrounding the exposed heme edge of cytochrome *c*, thereby providing a stable protein−electrode complex with an orientation suitable for electron transfer. This mechanism is analogous to the interactions between cytochrome *c* and its physiological redox partners.

In several cyclic voltammetric (CV) studies of cytochrome *c* at modified gold electrodes, the rate constant for the electron transfer has been reported after being determined using the method of Nicholson.[6] In a cyclic voltammetric experiment, the cathodic and anodic peaks for a reversible reaction are expected to be separated by 57/*n* mV.[7] The rate constant is determined by increasing the sweep rate to a range where the reaction becomes quasi-reversible so as to produce an increasing separation of the CV peaks with increasing sweep rate. The peak separation for cytochrome *c* at various modified electrodes is reported as ranging from 70 to 100 mV, depending on the modifier,[4] and the rate constants determined are reported as generally ranging from 10^{-3} to 10^{-4} cm s^{-1}. These values reported therefore imply quasi-reversibility of the reaction. Another indication of quasi-reversibility discussed in the literature[8] is a decrease in the slope of a peak current, i_p, vs the square root of sweep rate, $\nu^{1/2}$, with increasing sweep rate. Based on the reported rate constants for the reaction, this decrease in i_p should be noticeable yet linear i_p vs $\nu^{1/2}$ plots have been reported.[9]

Contrary to the CV results obtained at macroelectrodes, Bond and co-workers[9] have shown that at a 4,4′-bipyridal disulfide-modified gold microelectrode and rotating disk electrode a reversible Nernstian one-electron slope is obtained. Plots of the limiting current, i_L, vs the square root of the rotation rate, $\omega^{1/2}$, were linear, which also implies reversibility of the reaction.

The differences between the CV of proteins at "macro" and microelectrodes have been rationalized by assuming that the modified electrode containing electroactive binding sites is analogous to a microelectrode array.[9,10] If large numbers of these sites are blocked, then diffusion to "isolated" sites is radial and a sigmoidal response is expected. With large numbers of sites with little or no blocking, the diffusion layers overlap and the response is as for linear diffusion to a planar electrode with a 57/*n* mV peak separation for a reversible reaction. Blocking of the electroactive sites is presumed to be by denatured protein. In between these two limits, a mixture of the two diffusional modes prevails and the response is the sum of the current generated from the two modes resulting in CV peak separation which increases as blocking of surface sites increases, and eventually, the peaks flatten and become more sigmoidal in character with further blocking.

Büchi and Bond[11] applied the model of Gueshi et al.[12] for cyclic voltammetry at a partially blocked electrode to explain, among other things, the peak separation being >57/*n* mV for the reduction of cytochrome *c* at a carbon electrode. Simulations were done, and good correspondence between experimental and observed peak separation was obtained with a value of 8×10^{-7} cm^2 s^{-1} for the diffusion coefficient.

The diffusion coefficient of cytochrome *c*, calculated from CV data by plotting i_p vs $\nu^{1/2}$ at 4,4′-bipyridal disulfide-modified electrodes is generally found to be $6.5 \pm 0.5 \times 10^{-7}$ cm^2 s^{-1}. What is surprising about this value is that it is considerably smaller than the value of 11.1×10^{-7} (horse heart[13]) and 11.4×10^{-7} cm^2 s^{-1} (bovine heart[14]) reported in the biochemical literature. Values as high as 13.2×10^{-7} cm^2 s^{-1} have been

† E-mail: mikeh@gold.chem.hawaii.edu.

⊗ Abstract published in *Advance ACS Abstracts,* September 1, 1997.

S1089-5647(97)00742-6 CCC: $14.00

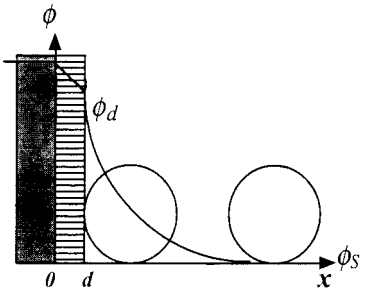

Figure 1. Potential profile with adsorbed monolayer on electrode.

reported[15] for bovine heart cytochrome *c*. Thus, values of the diffusion coefficient reported from CV experiments are more consistent with proteins with molecular weights four to five times that of cytochrome *c*.

In contrast to the values for the diffusion coefficient obtained from CV experiments at the 4,4′-bipyridal disulfide-modified gold electrode, at a bare gold electrode and an In_2O_3 electrode,[5] a value of $(11-12) \times 10^{-7}$ cm^2 s^{-1} has been reported. A similar value was obtained from RDE experiments at a 4,4′-bipyridine-modified gold electrode[16]. The diffusion coefficient in RDE experiments is calculated from the limiting current. While we do not consider the effect of monolayers on RDE experiments in this paper, the equation for the RDE limiting current does not contain potential terms, unlike the equation for the peak current in cyclic and linear sweep voltammetry. We would therefore not expect any change in the diffusion coefficient calculated from limiting current data due to the effects that we discuss below. We do note, however, that a lower value of 6.0×10^{-7} cm^2 s^{-1} has been reported at a 4,4′-bipyridal disulfide-modified rotating gold electrode.[9]

One aspect that has not been considered is how the potential drop across the modified layer effects the CV response. By virtue of having a modified layer present, the distance of closest approach of cytochrome *c* to the electrode is altered (Figure 1). This in turn effects the potential difference and hence the potential energy driving the reaction. Since potential difference across the cell will not be the same as the potential difference acting on the molecule at the distance of closest approach, then qualitatively one might expect some distortion of the CV, the amount of which would be dependent on the magnitude of the potential drop across the modified layer. In such a case, this may lead to the resultant increase in peak separation of the CV. Therefore, the effect that an adsorbed electroinactive monolayer has on a cyclic voltammogram has been investigated and reported in this paper based on the assumption that the monolayer is unblocked from adsorbed impurities or denatured protein. Following general remarks on the effect of monolayers on cyclic voltammetric response, the results for the reduction of cytochrome *c* at a 4,4′-bipyridal disulfide-modified gold electrode are discussed.

Theory

We envisage a reaction scheme in which the oxidized molecule diffuses from the bulk to the surface of an adsorbed monolayer of thickness *d* and assume that any interaction between the electroactive molecule and the surface of the adsorbed layer does not significantly retard or enhance the kinetics of electron transfer. It is also assumed that the effect of distance of closest approach *d* of the diffusing molecule on the reaction kinetics does not slow the reaction to the point where it is no longer reversible on the CV time scale. This condition is implied if the peak separation does not increase within a given range of sweep rates.

$$O^z_{x=\infty} \rightleftharpoons O^z_{x=d} \tag{1}$$

$$O^z_{x=d} + ne^- \rightleftharpoons R^{z-n}_{x=d} \tag{2}$$

$$R^{z-n}_{x=d} \rightleftharpoons R^{z-n}_{x=\infty} \tag{3}$$

It follows that at equilibrium

$$\mu^\circ_{O_d} + RT \ln a_{O_d} + zF\phi_d + n\mu_e^{\circ M} - nF\phi^M = \mu^\circ_{R_d} + RT \ln a_{R_d} + (z-n)F\phi_d \tag{4}$$

By taking the potential of the bulk solution, ϕ_S, as a zero reference point, and by substituting the concentration of O and R at $x = d$ for their activities, (4) is rearranged to give

$$E = E^{\circ\prime} + \phi_d + (RT/nF) \ln(c_{O_{x=d}}/c_{R_{x=d}}) \tag{5}$$

In the cyclic voltammetric experiment, the potential is swept linearly with time, causing the potential profile to be altered. The potential can therefore be expressed as a function of distance and time, i.e., $\phi(x,t)$, from which it follows that $\phi(0,t) = \phi_M$ and $\phi(\infty,t) = \phi_S$. The potential of the cell is expressed in terms of the initial potential and the sweep rate

$$E(t) = E_i - \nu t \tag{6}$$

Arrival at an expression for the cyclic voltammogram requires the solution of the equations for diffusion, a planar surface with the additional boundary conditions given in eqs 7−11.

$$\frac{\partial c_O(x,t)}{\partial t} = D_O \frac{\partial^2 c_O(x,t)}{\partial x^2} \quad \text{and} \quad \frac{\partial c_R(x,t)}{\partial t} = D_R \frac{\partial^2 c_R(x,t)}{\partial x^2} \tag{7}$$

$$c_O(x,0) = c_O^* \exp[-z_O F\phi(x,0)/RT] \quad \text{and} \quad c_R(x,0) = 0 \tag{8}$$

where c_O^* is the bulk concentration of the electroactive species.

$$\lim_{x\to\infty} c_O(x,t) = c_O^* \quad \text{and} \quad \lim_{x\to\infty} c_R(x,t) = 0 \tag{9}$$

and the current is defined as

$$i(t) = nFAD_O\left[\frac{\partial c_O(x,t)}{\partial x}\right]_{x=d} \tag{10}$$

if we assume that reaction 2 is electrochemically reversible so that the concentrations of O and R at $x = d$ can always be described by (5), then combining (5) and (6) and rearranging yields

$$c_O(d,t)/c_R(d,t) = \exp[(nF/RT)(E_i - \nu t - \phi(d,t) - E^{\circ\prime})] \tag{11}$$

where $\phi(d,t)$ can be derived from Figure 1

$$\phi(d,t) = \frac{(E - E_{pzc})C_m + z_m F\Gamma_m f}{C_m + C_{dif}} \tag{12}$$

E_{pzc} is the potential of zero charge of the electrode, Γ_m is the surface excess of the monolayer with charge z_m, f is the fraction of the adsorbed monolayer that is charged, and C_m and C_{dif} are the capacitances of the monolayer and the diffuse layers,

respectively. For a 1:1 *z*:*z* electrolyte of concentration c^*_{sup}, the diffuse capacitance, C_{dif}, is defined as

$$C_{dif} = \epsilon_o \epsilon \kappa \cosh[zF\phi(d,t)/2RT] \quad (13)$$

where $\kappa = (3.29 \times 10^7) z c^{*1/2}_{sup}$.[8] Equation 12 assumes that any charge existing due to the monolayer occurs at the monolayer−solution interface, that the monolayer is impenetrable to the solution so that a linear potential drop is expected across the monolayer, and that the charge on the monolayer is constant throughout the experiment. The solution to eqs 7−10 is

$$c_O(d,t) = c^*_O \exp[-z_O F\phi(x,0)/RT] - \frac{1}{(\pi D_O)^{1/2} nFA} \int_0^t \frac{i(\tau)}{\sqrt{(t-\tau)}} d\tau \quad (14)$$

$$c_R(d,t) = \frac{1}{(\pi D_R)^{1/2} nFA} \int_0^t \frac{i(\tau)}{\sqrt{(t-\tau)}} d\tau \quad (15)$$

Substituting (14) and (15) into (11) yields

$$\frac{nFA(\pi D_O)^{1/2} c^*_O \exp[-z_O F\phi(x,0)/RT]}{1 + (D_O/D_R)^{1/2} \exp[(nF/RT)(E_i - \nu t - \phi(d,t) - E^{\circ\prime})]} = \int_0^t \frac{i(\tau)}{\sqrt{(t-\tau)}} d\tau \quad (16)$$

Equation 16 can be rearranged to

$$\frac{1}{1 + \gamma\theta S(at)} = \int_0^{at} \frac{\chi(z)}{\sqrt{(at-z)}} dz \quad (17)$$

where

$$\chi(at) = i/nFA(\pi D_O)^{1/2} c^*_O \exp[-z_O F\phi(x,0)/RT] \quad (18)$$

$$a = nF\nu/RT \quad (19)$$

$$\gamma = (D_O/D_R)^{1/2} \quad (20)$$

$$\theta = \exp[(nF/RT)(E_i - \phi(d,t) - E^{\circ\prime})] \quad (21)$$

$$S(at) = \exp(-at) \quad (22)$$

Equation 17 can be solved numerically by first expressing ϕ in terms of a quadratic function of νt.

$$\phi(d,t) = m(\nu t)^2 + n(\nu t) + c \quad (23)$$

For electrolytes that are 0.1 M or higher, the correlation coefficient is $r > 0.999$ in the potential region $E_{pzc} \pm 500$ mV and $C_m < 15$ μF cm^{-2}. For more dilute solutions, a higher-order polynomial may be necessary but a solution can be obtained by following this procedure.

Substituting eq 23 into eq 17 and assuming for simplicity that $\gamma = 1$ yields (see Appendix)

$$\int_0^{at} \frac{\chi(z)\, dz}{\sqrt{at-z}} = \frac{1}{1 + \exp[(nF/RT)(E_i - \nu t - (m(\nu t)^2 + n(\nu t) + c) - E^{\circ\prime})]} \quad (24)$$

Equation 24 is an Abel integral equation. After solving this equation for $\chi(at)$, doing an integration by parts, noting that $(at)^{1/2}/2\pi \operatorname{sech}^2[(\ln \theta_c)/2] \approx 2/\theta_c (at/\pi)^{1/2}$ and multiplying by $\pi^{1/2}$ to allow comparison with the tabulated values of Nicholson and Shain,[7] yields (see Appendix)

$$\sqrt{\pi}\chi(at) = \frac{2(1+m)}{\theta}\sqrt{\frac{at}{\pi}} + \frac{1}{2\sqrt{\pi}} \int_0^{at} \sqrt{at-z}(2n/f) \times \operatorname{sech}^2\{[\ln\theta - (1+m)z - (nz^2/f)]/2\} + \begin{Bmatrix} [1+m+(2nz/f)]^2 \operatorname{sech}^2\{[\ln\theta - (1+m)z - (nz^2/f)]/2\} \\ \tanh\{[\ln\theta - (1+m)z - (nz^2/f)]/2\} \end{Bmatrix} dz \quad (25)$$

Experimental Section

All electrochemical measurements were made with a BAS 100B electrochemical analyzer (Bioanalytical Systems, West LaFayette, IN) using a three-electrode cell containing a modified gold working electrode of area 0.0201 cm^2, platinum counter electrode, and Ag/AgCl/ KCl (3M) reference electrode (all Bioanalytical Systems). The working electrode was polished with alumina paste, rinsed with deionized water, and sonicated in deionized water. Electrodes were modified by dipping into a 0.1 mM solution of 4,4′-bipyridal disulfide (Aldrich Chemical Co., Milwaukee, WI, sold as Aldrithiol) in ethanol for 60 min and then rinsed in deionized water. All experiments were carried out at room temperature, which was 18 ± 1 °C.

Cytochrome *c* (from horse heart, Sigma Chemical Co., St. Louis, MO) was purified[17] prior to use and used on the same day. In all experiments, a supporting electrolyte of 0.1 M $NaClO_4$ and 2 mM phosphate buffer (pH 6.8) was used.

Concentrations of cytochrome *c* solutions were determined spectrophotometrically using the extinction coefficient of ferrocytochrome *c* at 550 nm, $\epsilon_{550} = 28.4$ cm^{-1} mM^{-1}.[18]

Results and Discussion

General Remarks. (1) Determination of Conditions under Which $\phi(d,t)$ Is a Quadratic Function of νt. All calculations of $\phi(d,t)$ were made iteratively from eq 13. From eq 13 one sees that $\phi(d,t)$ depends on the experimental variables E_{pzc}, Γ_m is the surface excess of the monolayer with charge z_m, C_m and, from C_{dif}, nature and concentration of the supporting electrolyte. Calculations and simulations were made by assuming that the monolayer is uncharged. $\phi(d,t)$ was determined as a function of νt at monolayer capacitances of 3−15 μC cm^{-2} and E_{pzc} from −500 to +500 mV vs $E^{\circ\prime}$ in a 0.1 M 1:1 supporting electrolyte. Even for a large monolayer capacitance, $C_m \approx 15$ μC cm^{-2}, if the supporting electrolyte is sufficiently concentrated, the value of $\phi(d,t)$ can be described by a quadratic function of νt for a wide variety of E_{pzc} values; therefore, values of C_{dif} for a 1:1 0.1 M electrolyte were used in all simulations. This represents a system that is commonly used experimentally. For $C_m = 15$ μC cm^{-2}, the range of E_{pzc} values that produced a correlation coefficient of $r > 0.999$ was ± 300 mV vs $E^{\circ\prime}$; for $C_m = 13$, it was $E_{pzc} = \pm$ 400 mV vs E_{pzc}. These E_{pzc} ranges and $E_{pzc} = \pm$ 500 mV vs $E^{\circ\prime}$ for $C_m \leq 11$ were used in the simulations described below. In order to simulate CV peak shape under other experimental conditions, higher-order polynomials of νt could be chosen.

(2) Effect of $\phi(d,t)$ on Peak Shape. The anodic and cathodic peak heights determined for monolayer capacitances of 3, 5, 7, 9, 11, 13, and 15 μC cm^{-2} for the range of E_{pzc} listed above are shown in Figure 2. The anodic peak height was slightly larger than the cathodic peak height for $C_m \neq 0$; however, the difference never exceeded 0.1%, therefore only one set of data

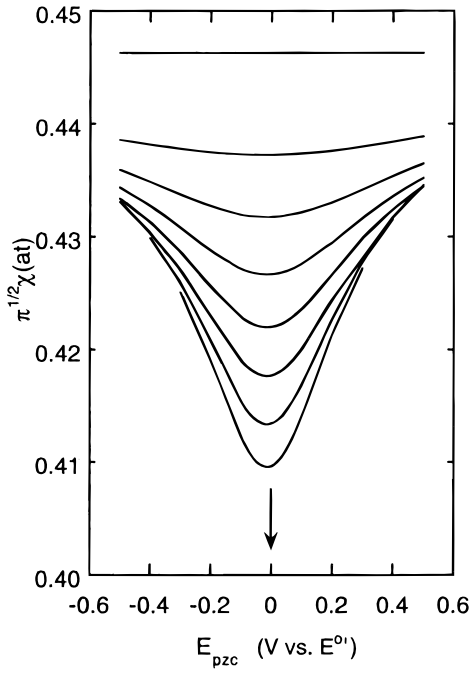

Figure 2. Plot of $\pi^{1/2}\chi(at)$ vs E_{pzc} for $C_m = 0$, 3, 5, 7, 9, 11, 13, and 15 μC cm^{-2} in 0.1 M 1:1 electrolyte.

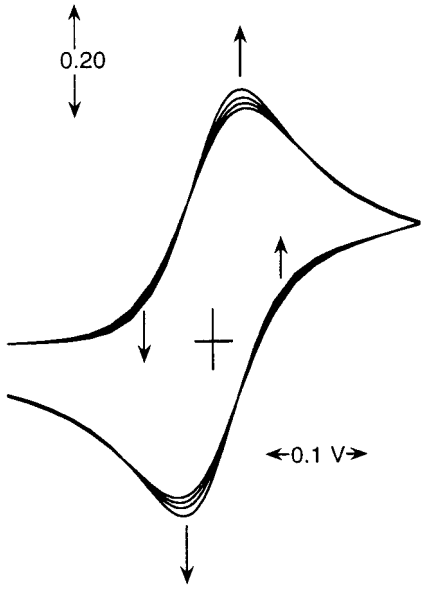

Figure 3. Simulated cyclic voltammograms for $E_{pzc} = 0$ for an electrode with monolayer with $C_m = 0$ (i.e., no monolayer), 5, 9, and 13 μC cm^{-2}.

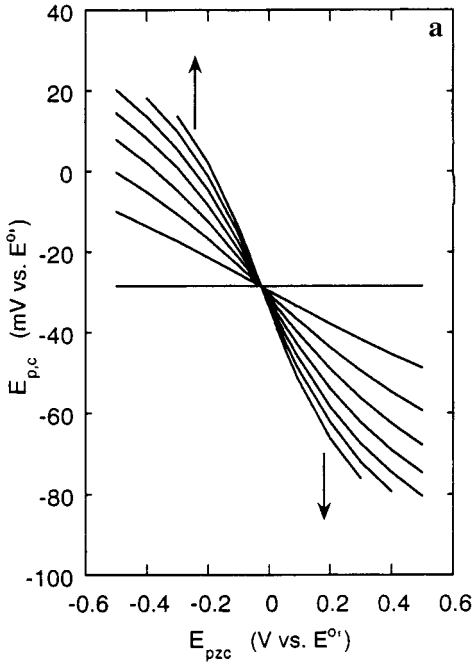

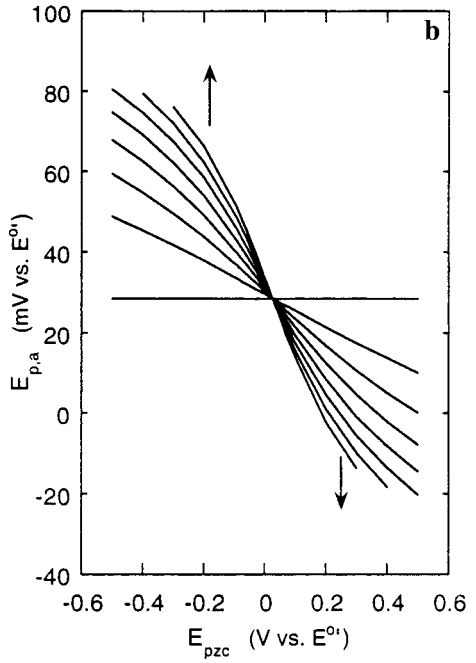

Figure 4. Shift in (a) cathodic and (b) anodic peak potentials as a function of E_{pzc}.

are shown. The results displayed in Figure 2 are somewhat counterintuitive in that the maximum decrease in peak height, relative to an ideal system with no monolayer, is observed when the E_{pzc} lies close to the formal potential.

Figure 3 shows some simulated cyclic voltammograms in which the decrease in the dimensionless current function with increasing capacitance is evident.

(3) Effect of $\phi(d,t)$ on Peak Potential. Figure 4 shows that as the E_{pzc} shifts anodically both the anodic and cathodic peak potentials shift in the cathodic direction; the magnitude of the shift becomes greater with increasing C_m. This reflects the decrease in $\phi(d,t)$ at the peak potential as the E_{pzc} shifts anodically. Therefore, for the reduction, the magnitude of the potential acting on the molecule at $x = d$, $E - \phi(d,t)$, is more anodic than the potential across the cell. Consequently, while a CV cathodic peak is expected at $-28.5/n$ mV (vs $E^{o\prime}$) for a reaction occurring at the surface of the electrode ($x = 0$), the true potential acting on a molecule at $x = d$ is anodic of this value, which causes the peak to be shifted cathodically. By the same reasoning, a molecule being oxidized on the reverse sweep, for which CV anodic peak is expected at $+28.5/n$ mV (vs $E^{o\prime}$) for a reaction occurring at the surface of the electrode ($x = 0$), is oxidized more easily at $x = d$ and therefore the peak is once again shifted cathodically. It is not surprising that the dependency of the peak potentials on $\phi(d,t)$ is

$$E_{p,c} = -0.0285 + \phi(d,t)_{\nu t = E_i - E_{p,c}} \quad (26)$$

$$E_{p,a} = 0.0285 + \phi(d,t)_{\nu t = E_i - E_{p,a}} \quad (27)$$

When the E_{pzc} is shifted in the cathodic direction, we find that the anodic and cathodic peaks shift anodically since this time

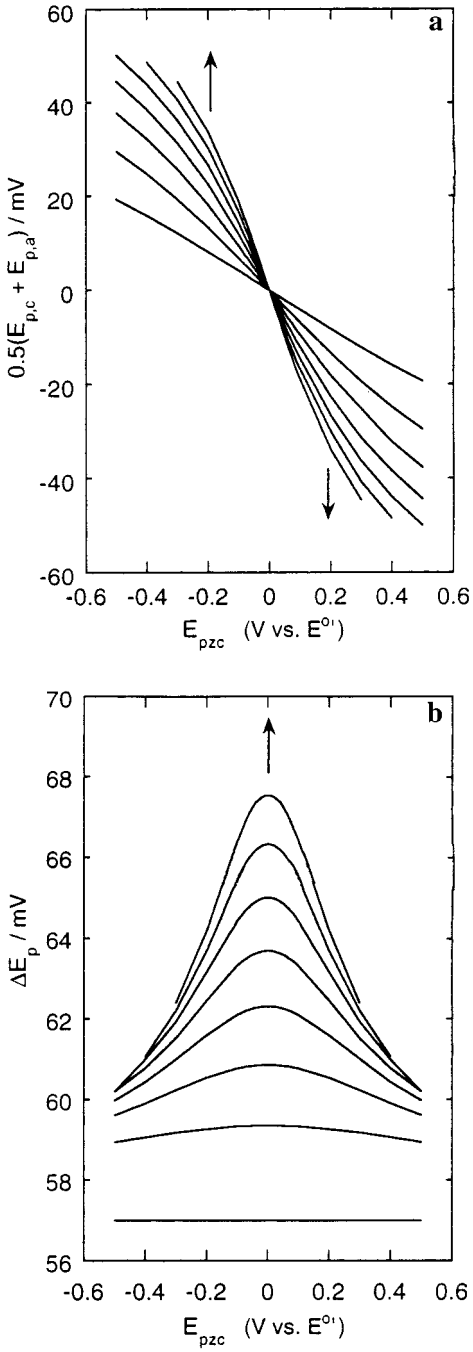

Figure 5. (a) Shift in midpoint between the cathodic and anodic peaks relative to $E^{\circ\prime}$. (b) Cathodic to anodic peak separation ΔE_p vs E_{pzc} for C_m = 0, 3, 5, 7, 9, 11, 13, and 15 μC cm^{-2} in 0.1 M 1:1 electrolyte.

the magnitude of the potential acting on the molecule at $x = d$, $E - \phi(d,t)$ is more cathodic than the potential across the cell.

It is common practice to assign the midpoint potential between the anodic and cathodic peak potentials as the formal potential; however, from the above discussion, this midpoint potential will be shifted, at times significantly, from the true formal potential. Figure 5 shows the anticipated shift in the midpoint potential relative to the formal potential.

It follows from this discussion that attempts to determine the rate constant for the monolayer covered electrodes based on the working curves method of Nicholson[6] will be subject to error since a requirement of that method is that the peak separation approaches 57/n mV for large rate constant values i.e., reversible systems.

Reduction of Cytochrome *c* at a 4,4′-Bipyridal Disulfide-Modified Gold Electrode. (1) Derivation of an Equation Specific for the Reduction of Cytochrome *c*. Equation 5 is derived by assuming electrical work term in eq 4 is due to point charges in a field. Cytochrome *c* is a protein with a heterogeneous charge distribution and has dimensions similar to those of the double layer. Given that the thickness of the double layer is insufficient to allow a concentration gradient, we have taken the initial concentration of cytochrome *c* at the surface of the monolayer as being equal to the bulk concentration. The initial boundary condition then becomes

$$c_O(d,0) = c_O^* \tag{28}$$

from which it follows that

$$i = nFA(\pi D_O)^{1/2} c_O^* \chi(at) \tag{29}$$

The fraction of the monolayer that was charged was calculated using eq 30, which was derived by Smith and White.[19]

$$\log[\Gamma_{HA^+}/\Gamma_A] = \log[f/(1-f)] = -\mathrm{pH} + \mathrm{p}K_a - [(E - E_{pzc})F/2.3RT] \tag{30}$$

where HA^+ and A refer to the conjugate acid and the base, respectively. Equation 30 was rearranged to give f, which was then substituted into (12).

The supporting electrolyte was not 1:1, due to the addition of buffer and cytochrome *c*. The following procedure was used to determine C_{dif}. The diffuse charge was calculated in the range -100 mV $< \phi(d,0) < +100$ mV using eq 31[20]

$$-\epsilon_o\epsilon\left(\frac{d\phi}{dx}\right)_{x=d} = \sigma_{dif} = \{2000\epsilon_o\epsilon RT\sum_i c_i[\exp(-z_iF\phi(d,t)/RT) - 1]\}^{1/2} \tag{31}$$

The calculated diffuse charge was then plotted against $\phi(d,0)$ and a fifth-order polynomial fitted ($r = 0.999$).

$$\sigma_{dif} = -0.7726\phi + (1.043 \times 10^{-4})\phi^2 - 40.46\phi^3 - (8.930 \times 10^{-3})\phi^4 - (4.694 \times 10^3)\phi^5 \tag{32}$$

The derivative of (32) was taken with respect to ϕ to give the diffuse capacitance as a function of ϕ.

$$-\frac{d\sigma_{dif}}{d\phi} = C_{dif} = 0.7726 - (2.086 \times 10^{-4})\phi + 121.4\phi^2 + (2.772 \times 10^{-2})\phi^3 + (2.347 \times 10^4)\phi^4 \tag{33}$$

Equation (33) was substituted into (12) for further calculations.

(2) Results and Verification. Figure 6 shows that experimentally the cyclic voltammograms of cytochrome *c* exhibited a peak separation greater than 57 mV although generally the peak separation was constant at $\nu \leq 300$ mV s^{-1}.

Occasionally an increase in peak separation with increasing sweep rate was observed. In light of the papers by Bond and co-workers[9−11] on the effect of adsorbed impurities or adsorption of denatured protein on the CV response, we interpreted this as an indication that our purification procedure had been unsuccessful. After the purification of cytochrome *c* with fresh ion exchange resin was repeated, peak separation was again constant in the sweep rate range mentioned. Some samples of purified protein that had exhibited no variation in peak separation were tested after four to seven days at 4 °C. After this storage period, CV peak separation began to increase with increasing sweep rate. All results reported are for solutions that were examined on the day of purification.

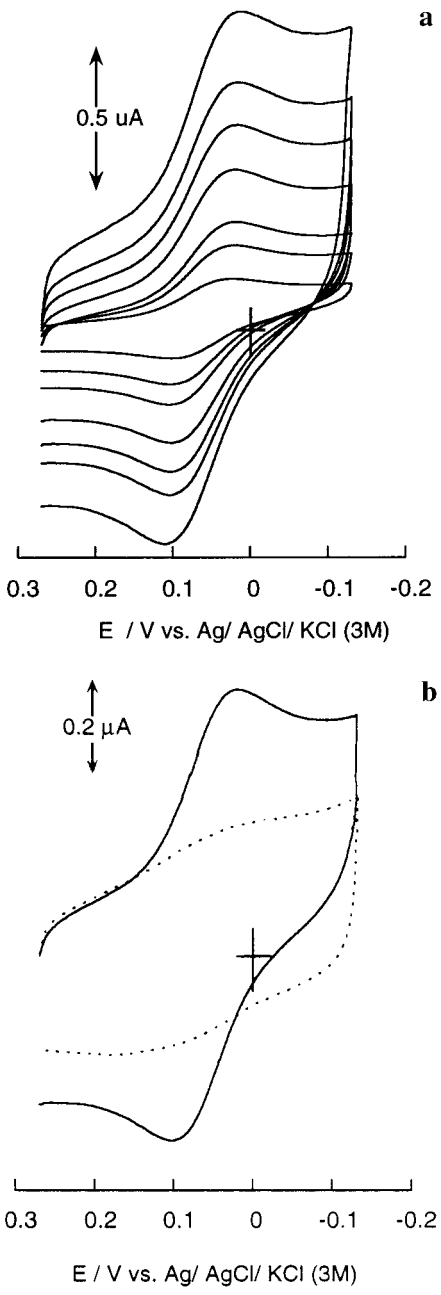

Figure 6. (a) Experimentally obtained CVs for the reduction of 177 μM cytochrome *c* in 0.1M $NaClO_4$ and 2 mM phosphate buffer (pH 6.8). Sweep rates: 10, 30, 50, 100, 150, 200, and 300 mV s^{-1}. Peaks increasing with increasing sweep rate. (b) (—) Same solution as (a) and (···) supporting electrolyte alone. Sweep rate 100 mV s^{-1}.

The cathodic peak height taken from CVs of a 177 μM solution of cytochrome *c* was plotted against the square root of the sweep rate ($\nu \leq 300$ mV s^{-1}), producing a line of best fit with equation $i = (6.98 \times 10^{-9} + 9.19 \times 10^{-7})\nu^{1/2}$ ($r = 0.9997$). Anodic and cathodic peak separation, ΔE_p, was 69 ± 4 mV with the midpoint at +276 mV vs NHE (Table 1).

Table 2 shows a list of the values obtained from the literature that were used in calculations. While the pK_a of a surface-confined group is potential dependent, as a first approximation it was assumed to be independent in the potential range of these experiments. Both the literature values for the pzc of polycrystalline gold were used in calculations for comparison. The reported value for the capacitance of a 4-mercaptopyridine monolayer (which forms from the adsorption of 4,4′-bipyridal disulfide on gold) is 35 μF cm^{-2}.[21] This value is rather high and may indicate that some solvent penetration of the monolayer occurred. Taking the N−S distance of ∼4.6 Å, the length of the S−Au bond of ∼2.3 Å and the dielectric of pyridine (ϵ = 12.3) gives an estimated monolayer capacitance of ∼16 μF cm^{-2}. The CVs obtained from supporting electrolyte indicated a capacitance of this order. Hence, both values for the monolayer capacitance were used in calculations.

TABLE 1: Anodic and Cathodic Peak Potential Data for the Reduction of Cytochrome *c* in 0.1 M $NaClO_4$ and 2 mM Phosphate Buffer (pH 6.8) at Different Scan Rates

sweep rate (mV s^{-1})	$E_{p,c} \pm 2$ mV	$E_{p,a} \pm 2$ mV	$\Delta E_p \pm 4$ mV
10	32	97	65
30	26	97	71
50	26	98	72
100	29	96	67
150	28	98	70
200	27	97	70
300	24	102	78

TABLE 2: List of Values Used in Calculations

parameter	literature value	reference
C_m[a]	35 μF cm^{-2}	21
	16 μF cm^{-2} [d]	
E_{pzc} of Au vs $E^{o\prime}$ [b]	−90 ± 100 mV	22
	−140 mV	23
Γ_m	0.67 nmol cm^{-2}	24
surface pK_a [c]	4.6 ± 0.5	21

[a] In 0.02 M $NaClO_4$ and 0.01 F Na_2CO_3. [b] $E^{o\prime}$ taken as +260 mV vs SHE.[18] [c] At +0.2 V vs Ag/AgCl(satd). [d] Estimated value (see text).

Table 3 shows the calculated results based on the literature values in Table 2 and the slope of the $i - \nu^{1/2}$ plot.

Considering the assumptions inherent in these calculations the predicted peak separation is in good agreement with that obtained experimentally by us, and others under similar experimental conditions, demonstrating that peak separations greater than 57/*n* mV occur in reversible systems. The value of the diffusion coefficient is in good agreement with literature values.

Taking C_m as 35 μF cm^{-2}, the corrected value of the formal potential is quite different from the literature value of +260 mV vs NHE. This is an indication of the sensitivity of the calculations of the corrected formal potential to the value of the pzc for the gold electrode at such a high monolayer capacitance. Better agreement with the literature value is obtained based on our estimate of C_m being ∼16 μF cm^{-2}. The calculated diffusion coefficient for cytochrome *c* is also in better agreement with literature values than previously reported from CV experiments.

Some variation between literature data for cytochrome *c* cyclic voltammetry may therefore be expected due to small variations in the pzc of the electrode and the monolayer capacitance between different groups of researchers.

Figure 7 shows a comparison between a baseline-subtracted CV of cytochrome *c* and that predicted by our model. The experimental baseline-subtracted CV current values were converted into their dimensionless form using the experimentally determined value for the diffusion coefficient given in Table 3 for $E_{pzc} = -90$ mV. The input variables for the two simulated CVs were $C_m = 0$ (no monolayer), $E^{o\prime} = +260$ mV vs NHE, $E_i = +200$ mV and $C_m = 16$ μF cm^{-2}, $E^{o\prime} = +254$ mV vs NHE, $E_i = +200$ mV, $E_{pzc} = -90$ mV.

One noticeable aspect of Figure 7 is that both simulated CVs fail to fit to the experimental baseline-subtracted CV on the rising portion of the CV. This reflects the difficulties in accurately performing a baseline subtraction on CVs obtained

TABLE 3: Calculated Data from CV Experiments with 177 μM Cytochrome *c* in 0.1 M $NaClO_4$ and 2 mM Phosphate Buffer (pH 6.8) for C_m of 35 and 16 μF cm^{-2} [a]

	E_{pzc} of Au (mV vs $E^{\circ\prime}$) [b]	$\chi(at)$	ΔE_p (mV)	$E^{\circ\prime}$ (mV vs NHE)	D ($\times 10^7$ cm^2 s^{-1})
calculated	−140	0.40689	66		
		(0.41781)	**(68)**		
calculated	−90	0.39187	70		
		(0.41540)	**(68)**		
calculated[c]		0.4463	57	276	8.8
experimental	−140		69 ± 4	232[d]	10.7
				(246)	**(10.1)**
experimental	−90		69 ± 4	242[d]	11.6
				(254)	**(10.2)**

[a] Values in parentheses are for 16 μF cm^{-2}. [b] $E^{\circ\prime}$ taken as +260 mV vs SHE.[18] [c] According to the model for cyclic voltammetry at a bare electrode. [d] The midpoint between the anodic and cathodic peaks of +276 mV vs NHE was "Corrected" by allowing for the supposed shift in the formal potential which is predicted by this model.

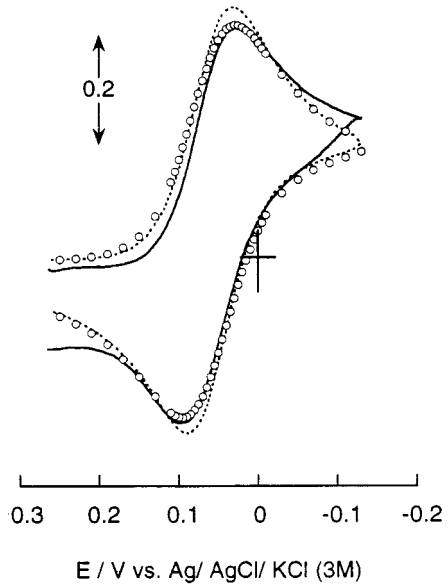

Figure 7. Comparison between baseline-subtracted experimental CV (—) and simulated CVs Parameters used for the conversion of the experimental current to a dimensionless form and the experimental conditions are described in text. Sweep rate 100 mV s^{-1}. Simulation parameters: (···) $C_m = 0$ (no monolayer), $E^{\circ\prime} = +260$ mV vs NHE, $E_i = +200$ mV; (○) $C_m = 16$ μF cm^{-2}, $E^{\circ\prime} = +254$ mV vs NHE, $E_i = +200$ mV, $E_{pzc} = -90$ mV.

from dilute solutions. In the regions of both the cathodic and anodic peaks, the larger currents produce a smaller percentage error in the subtraction procedure. In this region, a comparison can be made between the model and the experimental data.

On the scale used for reproducing Figure 7 in this journal, it is not immediately apparent that any differences in peak separation exist between the two simulated CVs given the broad nature of CV peaks. The peak separation for simulated CV for an electrode with no monolayer is 9 mV less than for an electrode with a monolayer of capacitance 16 μF cm^{-2}. The simulation using the model described in this paper does provide a good fit with the experimental data in the region of the CV peaks. The larger peak height observed for the simulated CV for an electrode with no monolayer contributes to the smaller diffusion coefficients reported when calculations have been based on the "classical" model.

In conclusion, both this work and other recent work[9] have failed to observe the increase in peak separation with increasing sweep rate that has frequently been reported. As a result of the work of Bond and co-workers, and from the results of this study, it seems likely that some of these earlier observations can be attributed to impurities in the solution resulting from an ineffectual purification procedure or storage of the sample prior to experimentation. In this study, a reversible CV response is observed for the reduction of cytochrome *c* at a 4,4′-bipyridal disulfide-modified gold electrode that is assumed to be unblocked, the general features of which may be predicted by the model presented.

Acknowledgment. This work was supported by NSF Grant CHE-9216304. We thank Dr. R. Larsen for his assistance with the purification of the cytochrome *c*.

Appendix

Equation 24 is an Abel integral equation. Assuming for simplicity that the diffusion coefficients are equal the solution to this equation is

$$\chi(at) = \frac{L(0)}{\pi\sqrt{at}} + \frac{1}{\pi}\int_0^{at} \frac{1}{\sqrt{at - z}}\left[\frac{dL(at)}{d(at)}\right]_{at=z} dz \quad \text{(A1)}$$

where

$$L(at) = \frac{1}{1 + \theta S(at)} \quad \text{(A2)}$$

Applying an integration by parts, i.e., $\int u(dv/dx)\,dx = uv - \int v(du/dx)\,dx$, to the integral term in (A1) with $(d/dz)(-2(at - 2)^{1/2}) = 1/(at - z)^{1/2}$, yields

$$\chi(at) = \frac{L(0)}{\pi\sqrt{at}} + \left\{\left[-\frac{2\sqrt{at - z}}{\pi}\left[\frac{dL(at)}{d(at)}\right]_{at=z}\right]_0^{at} + \frac{2}{\pi}\int_0^{at}\sqrt{at - z}\,\frac{d}{dz}\left[\frac{dL(at)}{d(at)}\right]_{at=z} dz\right\} \quad \text{(A3)}$$

At $at = 0$, $\chi(at) = 0$, and since when $at = 0$ the term in parentheses is zero, it follows that the integration constant must be $-(L(0)/\pi(at)^{1/2})$; therefore

$$\chi(at) = \frac{2\sqrt{at}}{\pi}\left[\frac{dL(at)}{d(at)}\right]_{at=0} + \frac{2}{\pi}\int_0^{at}\sqrt{at - z}\,\frac{d}{dz}\left[\frac{dL(at)}{d(at)}\right]_{at=z} dz \quad \text{(A4)}$$

$$\int_0^{at}\frac{\chi(z)\,dz}{\sqrt{at - z}} = \frac{1}{1 + \exp[(nF/RT)(E_i - \nu t - (m(\nu t)^2 + n(\nu t) + c) - E^{\circ\prime})]} \quad (24)$$

Taking the derivative of (A2) yields

$$\left[\frac{dL(at)}{d(at)}\right] = \frac{1}{4}[1 + m + (2nat/f)]\ \mathrm{sech}^2\{[\ln\theta - (1+m)at - (n(at)^2/f)]/2\} \quad \text{(A5)}$$

and the derivative of (A5) at $at = z$ is

$$\frac{d}{dz}\left(\frac{1}{4}[1 + m + (2nat/f)]\ \mathrm{sech}^2\{[\ln\theta - (1+m)at - (n(at)^2/f)]/2\}\right) = \frac{n}{2f}\mathrm{sech}^2\{[\ln\theta - (1+m)at - (n(at)^2/f)]/2\} + \frac{1}{4}\times \begin{Bmatrix}[1+m+(2n(at)/f)]^2\mathrm{sech}^2\{[\ln\theta - (1+m)at - (n(at)^2/f)]/2\} \\ \tan\{[\ln\theta - (1+m)at - (n(at)^2/f)]/2\}\end{Bmatrix} \quad \text{(A6)}$$

and substituting into (A4), noting that $((at)^{1/2}/2\pi)\ \mathrm{sech}^2[(\ln\theta_c)/2] \approx (2/\theta_c)(at/\pi)^{1/2}$ and multiplying by $\pi^{1/2}$ yields eq 25.

References and Notes

(1) Bond, A. M.; Hill, H. A. O.; Page, D. J.; Psalti, I. S. M.; Walton, N. J. *Eur. J. Biochem.* **1990**, *191*, 737−742 and references therein.

(2) Bond, A. M. *Anal. Proc.* **1992**, *29*, 132−148 and references therein.

(3) Bond, A. M. *Inorg. Chim. Acta* **1994**, *226*, 293−340 and references therein.

(4) Allen, P. M.; Hill, H. A. O.; Walton, N. J. *J. Electroanal. Chem.* **1984**, *178*, 69−86.

(5) Bowden, E. F.; Hawkridge, F. M.; Blount, H. N. *J. Electroanal. Chem.* **1984**, *161*, 355−376.

(6) Nicholson, R. S. *Anal. Chem.* **1965**, *37*, 1351−1355.

(7) Nicholson, R. S.; Shain, I. *Anal. Chem.* **1964**, *36*, 704−723.

(8) Bard, A. J.; Faulkner, L. R. *Electrochemical Methods*; J. Wiley & Sons, Inc.: New York, 1980; p 412.

(9) Bond, A. M.; Hill, H. A. O.; Komorsky-Lovric, S.; Lovric, M.; McCarthy, M. E.; Psalti, I. S. M.; Walton, N. J. *J. Phys. Chem.* **1992**, *96*, 8100−8105.

(10) Armstrong, F. A.; Bond, A. M.; Hill, H. A. O.; Psalti, I. S. M.; Zoski, C. G. *J. Phys. Chem.* **1989**, *93*, 6485−6493.

(11) Büchi, F. N.; Bond, A. M. *J. Electroanal. Chem.* **1991**, *314*, 191−206.

(12) Gueshi, T.; Tokuda, K.; Matsuda, H. *J. Electroanal. Chem.* **1979**, *101*, 29−38.

(13) Fling, M.; Horowitz, N. H.; Heinemann, S. F. *J. Biol. Chem.* **1963**, *238*, 2045−2053.

(14) Ehrenberg, A. *Acta Chem. Scand.* **1957**, *11*, 1257−1270.

(15) Nozaki, M. *J. Biochem. (Tokyo)* **1960**, *47*, 592−599.

(16) Albery, W. J.; Eddowes, M. J.; Hill, H. A. O.; Hillman, A. R. *J. Am. Chem. Soc.* **1981**, *103*, 3904−3910.

(17) Brautigan, D. L.; Ferguson-Miller, S.; Margoliash, E. *Methods Enzymol.* **1978**, *53*, 128−164.

(18) Sagara, T.; Koide, T.; Saito, H.; Akutsu, H.; Niki, K. *Bull. Chem. Soc. Jpn.* **1992**, *65*, 424−429.

(19) Smith, C. P.; White, H. S. *Langmuir* **1993**, *9*, 1−3.

(20) Hunter, R. J. *Zeta Potential in Colloid Science Principles and Applications*; Academic Press: London, 1981; p 28.

(21) Bryant, M. A.; Crooks, R. M. *Langmuir* **1993**, *9*, 385−387.

(22) Becka, A. M.; Miller, C. J. *J. Phys. Chem.* **1993**, *97*, 6233−6239.

(23) Anderson, T. N.; Anderson, J. L.; Eyring, H. *J. Phys. Chem.* **1969**, *73*, 3562−3570.

(24) Gui, J. H.; Lu, F.; Stern, D. A.; Hubbard, A. T. *J. Electroanal. Chem.* **1990**, *292*, 245−255.